Supplementary Figures

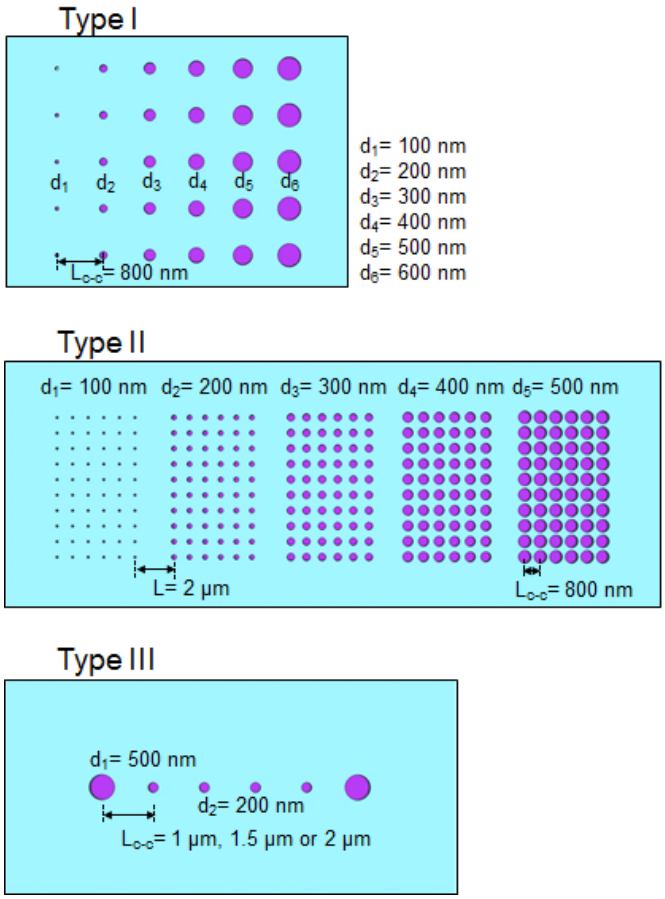

Supplementary Figure 1 | Schematics illustrating configurations of ZnO rod arrays. Configurations and parameters of circular hole arrays in PMMA growth masks used for Fig. 1a-c (type I), Fig. 2a and 2b (type II), and Fig. 3c and 3d (type III).

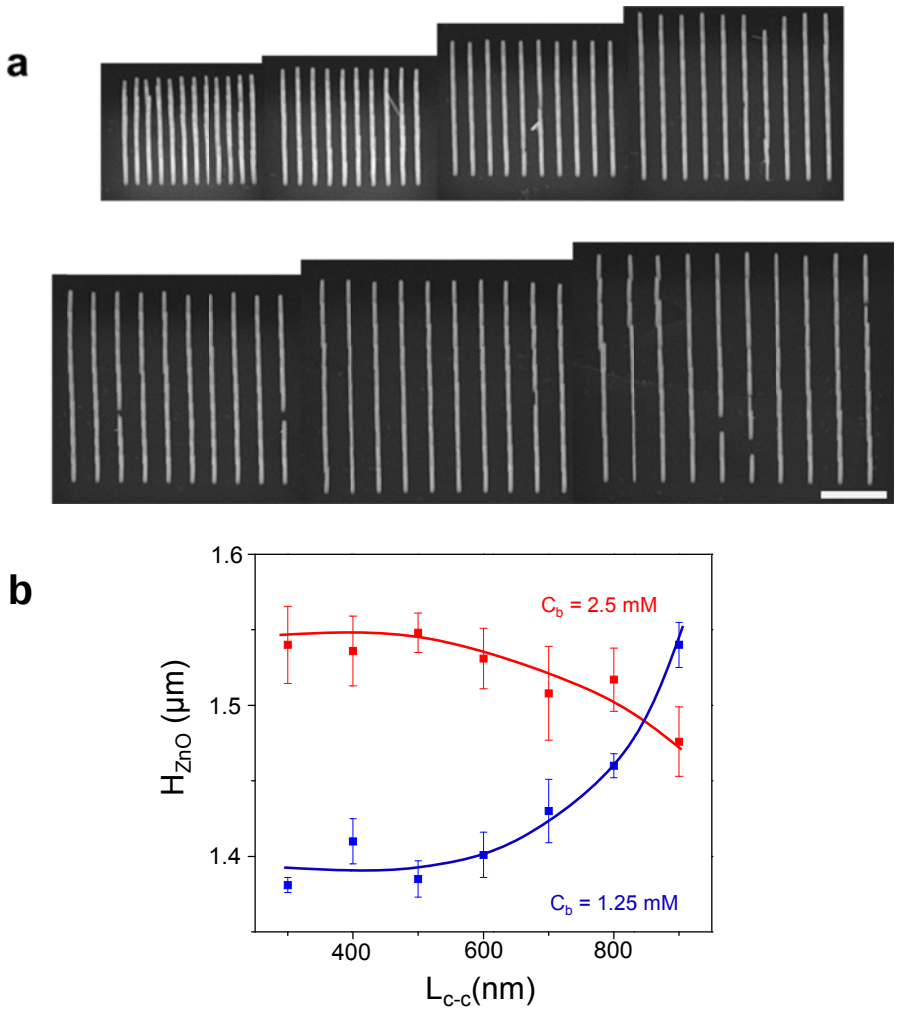

Supplementary Figure 2 | Analysis of H_{ZnO} as a function of L_{c-c}. (**a**) SEM images (70º tilt view) of ZnO *h*-rod arrays (10x10) with a constant D_{ZnO} of 160 nm and increasing L_{c-c} from 300 to 900 nm, grown at a C_b of 2.5 mM. Scale bars are 2 µm. (**b**) By increasing L_{c-c}, the H_{ZnO} decreased (at C_b of 2.5 mM, red squares) or increased (at C_b of 1.25 mM, blue squares), due to either synergetic effects or source competition among neighboring rods, respectively.

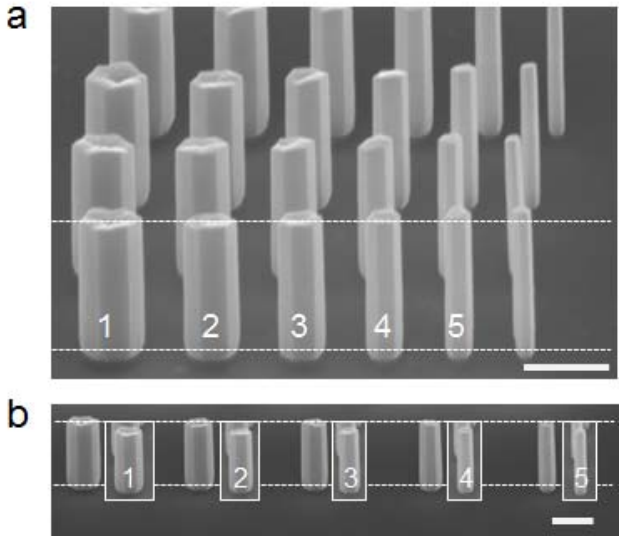

Supplementary Figure 3 | Synergetic effect versus completion effect. (**a,b**) SEM images (70º tilt view) of ZnO rod arrays grown with identical patterns to those used for Fig. 3a and b, but at a C_b of 1.6 mM. In this case, overall H_{ZnO} values are lower for an $L_{c\text{-}c}$ of 800 nm (**a**) than for an $L_{c\text{-}c}$ of 3 μm (**b**), owing to the competition effect prevailing over the synergetic effect, which is contrary to the case of Fig. 3. For direct comparison, each image of rods in (**a**) is inserted right after the corresponding rods with the same diameters (white boxes in (**b**)). Scale bars are 1 μm.

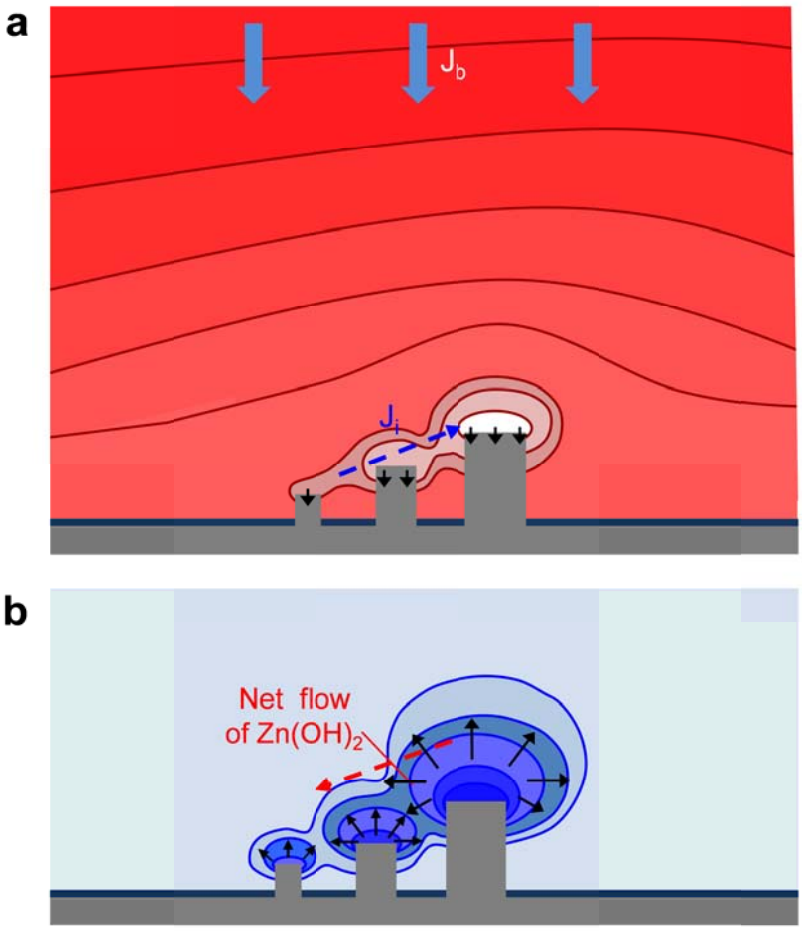

Supplementary Figure 4 | Geometries of mass-transport fields. Schematics illustrating the concentration profiles of the reactant precursor ions (Zn^{2+}) (**a**) and the intermediate species (the $Zn(OH)_2$) (**b**).

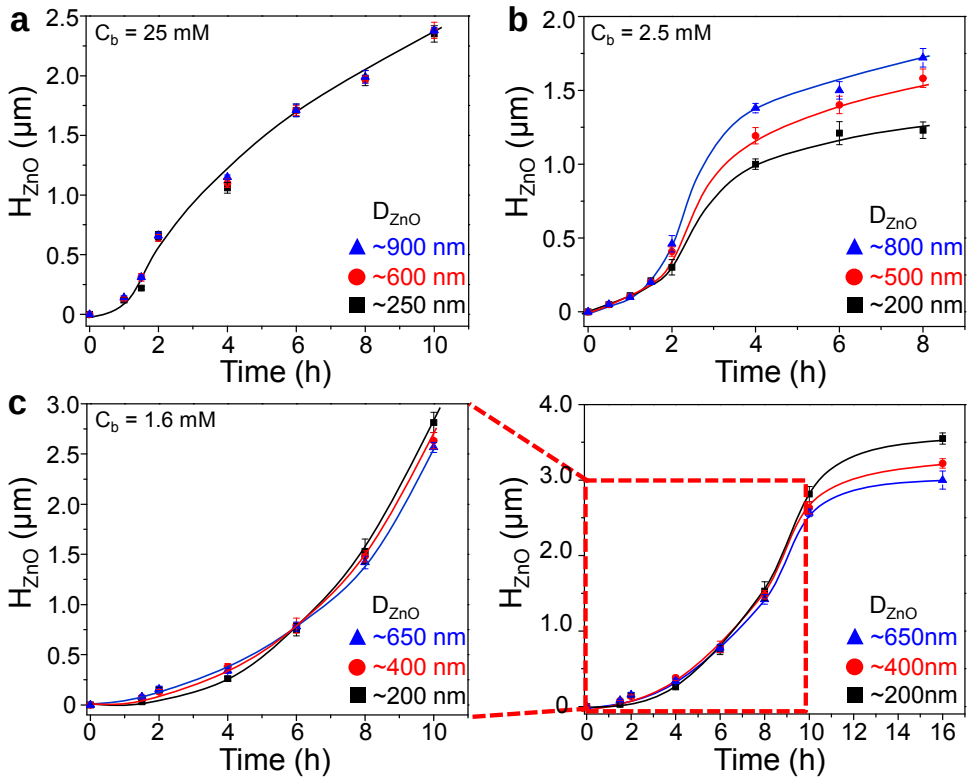

Supplementary Figure 5 | Analysis of time-dependent growth behaviors. (**a-c**) The height of ZnO rods (H_{ZnO}) as a function of growth time (t) at C_b values of 25 mM (**a**), 2.5 mM (**b**) and 1.6 mM (**c**). The diameters of ZnO rods (D_{ZnO}) were measured at t = 6 h. In all three cases, the growth rate is relatively slow at the initial stage (t < 1–2 h), due to the nucleation barrier and/or diffusion barrier created by the PMMA holes. Then, at t > ~2 h, the growth rate becomes faster and stabilized, depending on precursor concentration.

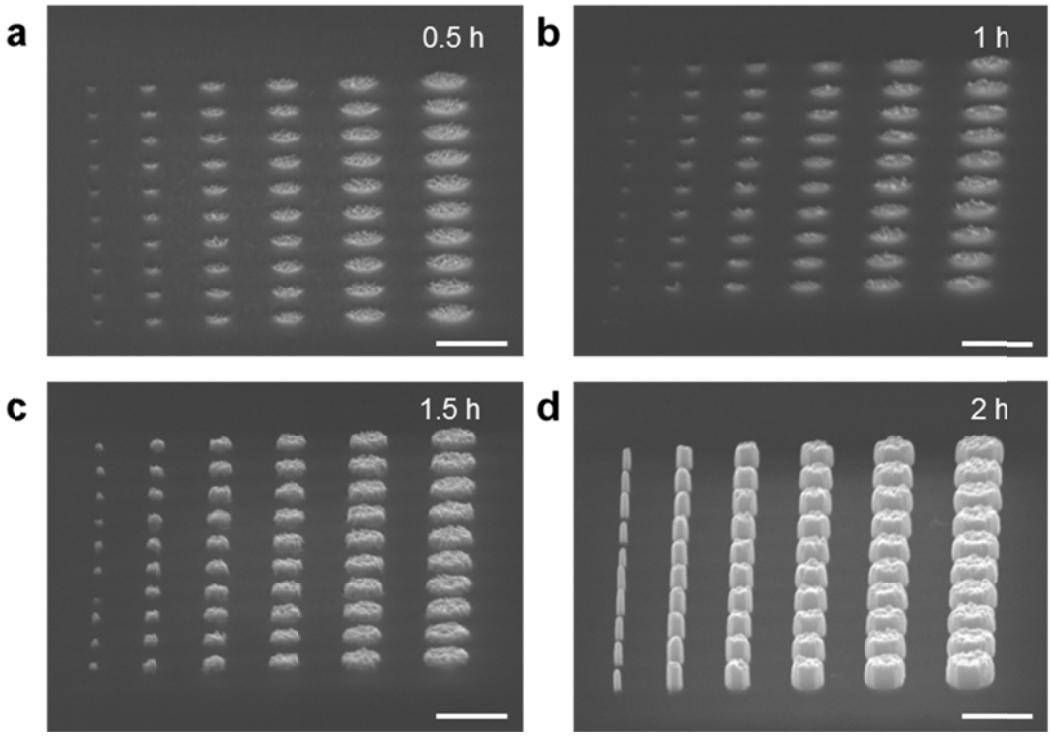

Supplementary Figure 6 | Time-evolution of ZnO rods growth at the early stage. A series of SEM images (70º tilt view) at t = 0.5 h (**a**), 1 h (**b**), 1.5 h (**c**) and 2 h (**d**). C_b is 2.5 mM. Scale bars are 1 μm.

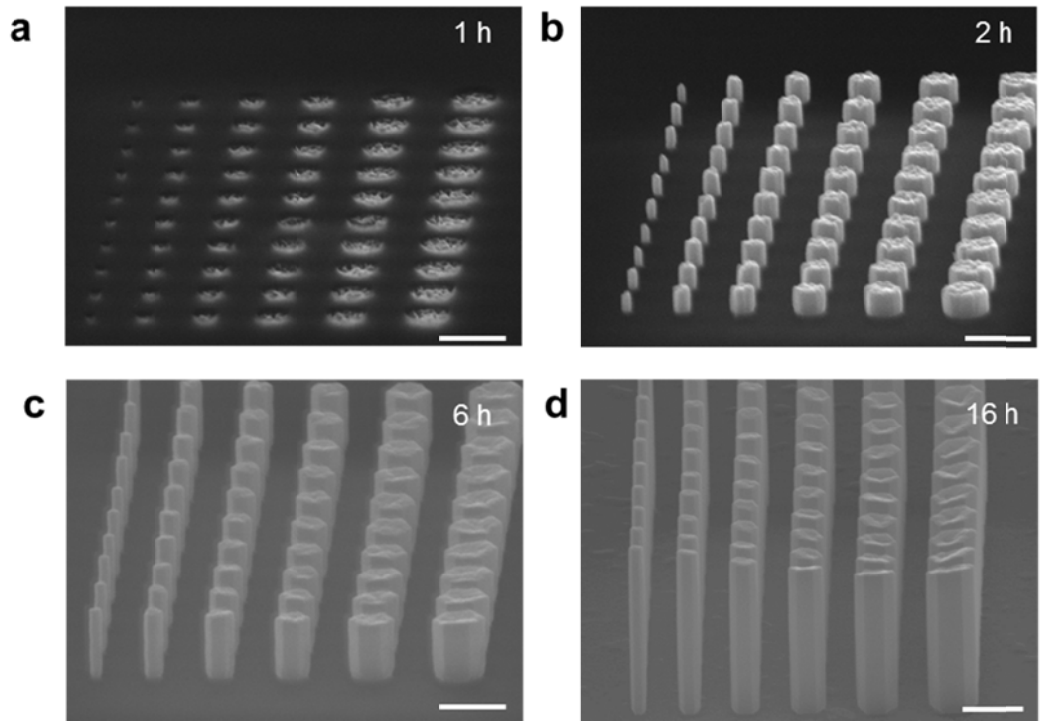

Supplementary Figure 7 | Time-evolution of ZnO nanorods growth with different times. SEM images (70º tilt view) of ZnO rod arrays at t = 1 h (**a**), 2 h (**b**), 6 h (**c**), and 16 h (**d**). C_b is 1.6 mM. Scale bars are 1 μm. The growth rate at the edge of the rod array (the thickest rods) in (**c**,**d**) is higher than that of the adjacent rods at the inside. This higher growth rate at the edge has the same origin as the formation of the concave tips of the thick rods.

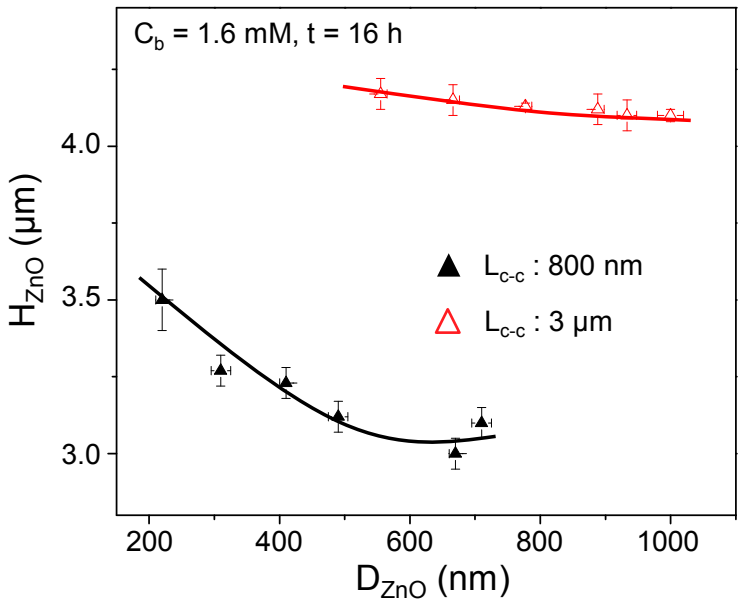

Supplementary Figure 8 | Analysis of growth behavior. Plots of H_{ZnO} versus D_{ZnO} for the ZnO rods grown at C_b = 1.6 mM and t = 16 h. The slope of H_{ZnO} versus D_{ZnO} curve in L_{c-c} of 800 nm is much larger than that in L_{c-c} of 3 μm, due to the significant source competition in smaller L_{c-c}. This feature is different from the case in Fig. 1f (t = 8 h), in which the slopes are similar in both L_{c-c} of 800 nm and 3 μm; the contribution of the GT effect is still active in L_{c-c} of 800 and counteracts the competition effect. As the growth time increases, the contribution of the GT effect decreases while the competition effect becomes more dominant. Thus, the H_{ZnO}/D_{ZnO} rate is much larger in smaller L_{c-c} at t = 16 h.

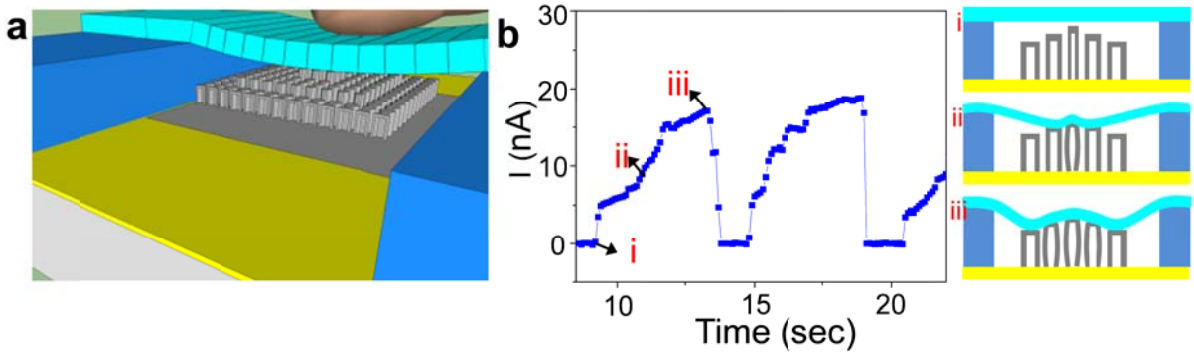

Supplementary Figure 9 | Nano-strain gauge. (**a**) Cross-sectional schematics of nano-strain gauge (or pressure sensor) based on 3D Si nanotube array. (**b**) The strain gauge shows a sensitive response to the application of pressure. A step-wise increase of current was demonstrated based on (i) no touch, (ii) imperceptible touch (~3–7 kPa), and (iii) gentle touch (~10 kPa), due to the unique height profile of Si nanotubes.

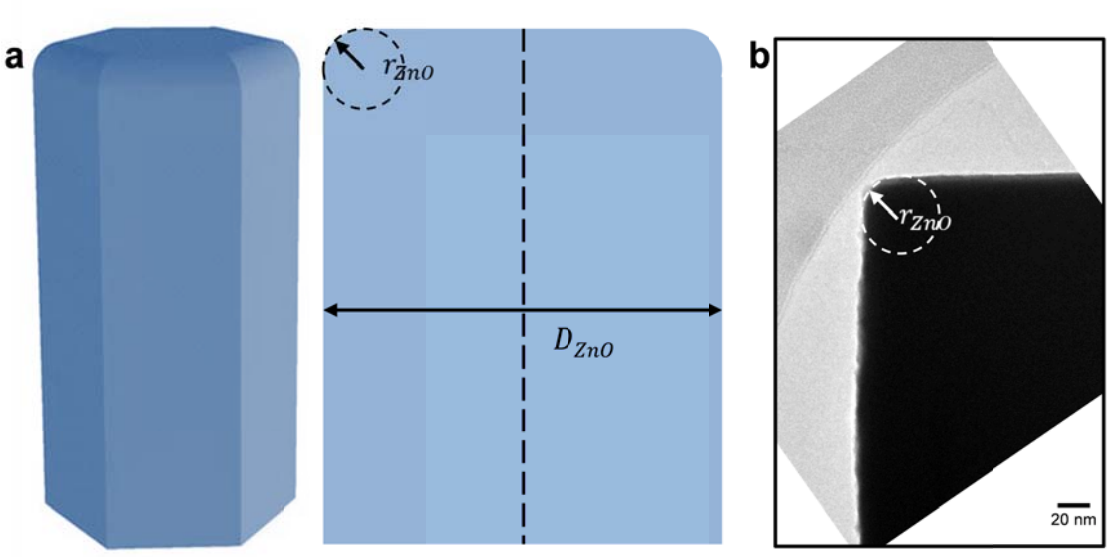

Supplementary Figure 10 | Analysis of a ZnO rod tip. (**a**) 3D and cross-sectional schematics of a ZnO hexagonal rod. The top surface of ZnO is flat at the center and the edge is rounded with a radius curvature r_{ZnO}. (**b**) TEM image at the edge of ZnO rod tip.

Supplementary Methods

Numerical analysis of the ratio between local diffusion and bulk diffusion of Zn^{2+} ion

In this analysis, the following are assumed: (1) Homogeneous reactions do not occur near the substrate, (2) Since OH^- ions are plentiful in water solutions, the growth rate is determined by the Zn^{2+} ion precursor, (3) Only axial growth is considered (lateral growth is ignored) and consumption of Zn^{2+} precursor occurs through reactions on the top (0001) surface that lead to vertical growth, and (4) The precursor ion concentration in the boundary layer drops linearly from a bulk concentration C_{bi} to an equilibrium concentration near the liquid/solid interface, C_{si}. In quasi-steady state conditions, the bulk diffusion of Zn^{2+} ions for the ideal 1D flux, J_b^{1D}, driven by the concentration gradient through the stagnant boundary layer is given by[1]

$$J_b^{1D} = D\frac{(C_{bi}-C_{si})}{\delta} = h_b(C_{bi} - C_{Si}) \qquad (1)$$

where D is the diffusion coefficient, δ is the boundary layer thickness, and C_i and C_s are bulk concentrations of Zn^{2+} ions and the concentration of Zn^{2+} ions on a flat ZnO crystal surface, respectively. The mass-transfer coefficient in the liquid-phase, h_b, is given by $h_b = -D/\delta$. The consumption rate of Zn^{2+} ions through the reaction taking place at the top (0001) surface is proportional to C_s, that is

$$J_s = k_s C_{Si} \qquad (2)$$

where k_s is the first-order rate constant for surface reaction on the top (0001) surface. In the steady state, $J_i^{1D} = J_s$, so by combining Eq. (1) and (2), we obtain

$$C_{si} = \frac{C_{bi}}{1+k_s/h_b} = \frac{C_{bi}}{1+\Phi} \qquad (3)$$

where Φ is the Thiele modulus[2], a measure of the ratio of surface reaction rate to rate of diffusion through the boundary layer. When the Φ is large ($\Phi > 1$), diffusion usually limits the overall growth rate; when $\Phi < 1$, the surface reaction is usually rate-limiting. By substituting C_{bi} from Eq. (3) to Eq. (1), J_b can be rearranged as a function of C_{si} and Φ:

$$J_b^{1D} = D\frac{C_{si}\Phi}{\delta} \qquad (4)$$

In case of isolated ZnO rods, the diffusion of the precursor ions, J_b, is larger than the value

of the ideal 1D flux, due to the contribution of diffusion from the side[3]. By comparing the height of a well-isolated ZnO rod with that of hexagonally closed-packed ZnO rods over the large area (> 0.5 x 0.5 cm^2)[4], we have calibrated the J_b as $J_b = n \cdot J_b^{1D}$, where the correction factor n was estimated to be ~4.

On the other hand, the local concentration of Zn^{2+} ion species in equilibrium near the nanoscale crystals is dependent on the local curvature of the solid phase. According to the Gibbs-Thomson effect, local equilibrium concentration C_{si}^{r} near the top (0001) surface of a rod with a radius curvature r_{ZnO} increases to

$$C_{si}^{r} = C_{Si}\exp\left(\frac{2\gamma V_m}{RT}\frac{1}{r_{ZnO}}\right) \qquad (5)$$

where γ is the interfacial energy, V_m is the molar volume of the solid phase, R is the gas constant, and T is the temperature. Considering only first-order terms (i.e., small deviations from the bulk concentration), it can be rewritten as

$$C_{si}^{r} = C_{Si} + \left(\frac{2\gamma V_m C_{si}}{RT}\frac{1}{r_{ZnO}}\right) \qquad (6)$$

As confirmed by a TEM image (Supplementary Fig. S10), the top surface of ZnO is composed of central flat surface and round edge with a radius curvature r_{ZnO}. r_{ZnO} is much smaller than the radius of ZnO rod, $D_{ZnO}/2$ (i.e., $r_{ZnO} << D_{ZnO}/2$). Considering the uniform growth along the axial direction, it is assumed that the local concentration near the top surface of ZnO rod becomes uniform, and the average value of the local concentration increment ($\overline{\Delta C_{si}^{D_{ZnO}}}$) at the diameter of ZnO rods is given by

$$\overline{\Delta C_{si}^{D_{ZnO}}} = \left(\frac{2\gamma V_m C_{Si}}{RT}\times\frac{1}{r_{ZnO}}\right)\times\frac{A_r}{A_t} \approx \left(\frac{2\gamma V_m C_{Si}}{RT}\times\frac{1}{r_{ZnO}}\right)\times\left(\frac{\left(\frac{1}{\sqrt{3}}D_{ZnO}\times 6\right)\times\left(\frac{1}{4}\times 2\pi r_{ZnO}\right)}{\left(\frac{1}{2}D_{ZnO}\times\frac{1}{\sqrt{3}}D_{ZnO}\right)\times 3}\right)$$

$$= \frac{4\gamma V_m C_{si}}{RT}\frac{\pi}{D_{ZnO}}$$

where A_t and A_r are the areas of total top surface and round edge of the ZnO rod tip, respectively. Note that $\overline{\Delta C_{si}^{D_{ZnO}}}$ is inversely proportional to D_{ZnO}, and is not affected by r_{ZnO}.

If we consider a thick rod 'A' with a diameter of D_{ZnO}^{A} and a thin rod 'B' with a diameter of D_{ZnO}^{B} separated by $L_{c\text{-}c}$, the local equilibrium concentrations near rods A and B can be written:

$$\overline{C_{si}^{A}} = C_{Si} + \left(\frac{4\gamma V_m C_{si}}{RT}\frac{\pi}{D_{ZnO}^{A}}\right) \qquad (7)$$

$$\overline{C_{si}^{B}} = C_{Si} + \left(\frac{4\gamma V_m C_{si}}{RT}\frac{\pi}{D_{ZnO}^{B}}\right) \qquad (8)$$

Since the $\overline{C_{si}^{A}} < \overline{C_{si}^{B}}$ local diffusion of the Zn^{2+} ion species from the region of the thin rod B to the region of thick rod A occurs, and the corresponding flux of the ions arriving on the top surface of rod A can be obtained according to Fick's first law:

$$J_i = -D\frac{(\overline{C_{si}^{A}} - \overline{C_{si}^{B}})}{L_{c-c}}\left(\frac{S_B}{S_A}\right) \qquad (9)$$

where the S_B/S_A is the ratio of surface area between rod B and rod A and given by $\frac{S_B}{S_A} = \left(D_{ZnO}^{B}/D_{ZnO}^{A}\right)^2$, which accounts for mass conservation. By substituting the $\overline{C_{si}^{A}}$ and $\overline{C_{si}^{B}}$ in Eqs. (7) and (8) into Eq.(9), J_i can be rearranged as

$$J_i = -\frac{D}{L_{c-c}}\frac{4\gamma V_m C_{si}\pi}{RT}\left(\frac{1}{D_{ZnO}^{A}} - \frac{1}{D_{ZnO}^{B}}\right)\left(\frac{D_{ZnO}^{B}}{D_{ZnO}^{A}}\right)^2 \qquad (10)$$

Finally, combining Eqs. (4) and (10), J_i/J_b versus Φ can be expressed as a function of D_{ZnO} and $L_{c\text{-}c}$:

$$\frac{J_i}{J_b} = \frac{\delta}{L_{c-c}}\frac{4\gamma V_m \pi}{RTn}\left(\frac{1}{D_{ZnO}^{B}} - \frac{1}{D_{ZnO}^{A}}\right)\left(\frac{D_{ZnO}^{B}}{D_{ZnO}^{A}}\right)^2\left(\frac{1}{\Phi}\right) \qquad (11)$$

Figure 4 shows the calculation result for the ratio of J_i to J_b for the adjacent rods with D_{ZnO} values of 800 nm and 140 nm, separated by $L_{c\text{-}c}$ values of 1, 2, and 3 μm. In this calculation, a value for the interfacial energy γ of 0.24 J/m^2 and the molar volume V_m of 14.8 cm^3/mol is used[5]. For the boundary layer thickness, δ, a typical diffusion length of Zn^{2+} ions in solution (~300 μm) was assumed.

Supplementary References

1 Ohring, M. *Materials science of thin films*. (Academic press, 2001).

2 Weintraub, B., Zhou, Z., Li, Y. & Deng, Y. Solution synthesis of one-dimensional ZnO nanomaterials and their applications. *Nanoscale* **2**, 1573-1587 (2010).

3 Boercker, J. E., Schmidt, J. B. & Aydil, E. S. Transport Limited Growth of Zinc Oxide Nanowires. *Cryst. Growth Des.* **9**, 2783-2789 (2009).

4 Kim, S. B. *et al.* Simple, Large-Scale Patterning of Hydrophobic ZnO Nanorod Arrays. *ACS Applied Materials & Interfaces* **4**, 3910-3915 (2012).

5 Wong, E. M., Bonevich, J. E. & Searson, P. C. Growth kinetics of nanocrystalline ZnO particles from colloidal suspensions. *J. Phys. Chem. B* **102**, 7770-7775 (1998).